Available online at www.sciencedirect.com

SciVerse ScienceDirect

Ceramics International 39 (2013) 8429–8439

CERAMICS INTERNATIONAL

www.elsevier.com/locate/ceramint

Synthesis of Cu^{2+} and Ag^{+} doped $Na_2Ti_3O_7$ by a facile ion-exchange method as visible-light-driven photocatalysts

M. Vithal*, S. Rama Krishna, G. Ravi, Suresh Palla, Radha Velchuri, Someshwar Pola

Department of Chemistry, Osmania University, Hyderabad 500007, Andhra Pradesh, India

Received 11 March 2013; received in revised form 7 April 2013; accepted 8 April 2013
Available online 28 April 2013

Abstract

Nano-sized Cu^{2+} and Ag^{+} doped sodium trititanate ($Na_2Ti_3O_7$) were prepared by a facile acid-free ion-exchange method in an aqueous solution at room temperature. All the samples were characterized by TGA, FESEM, EDS, Powder-XRD, UV–visible DRS and FT-IR spectroscopic methods. Both Cu^{2+} and Ag^{+} doped $Na_2Ti_3O_7$ were crystallized in monoclinic lattice with $P2_1/m$ space group. The band gap energies of all the samples were deduced from their UV–visible DRS profiles. Visible light-induced photocatalytic oxidation of the methylene blue (MB) dye has been examined in the presence of all the trititanates aqueous dispersion. The Ag^{+} doped trititanate exhibited remarkable photocatalytic activity in the degradation of methylene blue (MB) dye under visible light irradiation. Photochemical degradation of cyclohexa-1,4-diene and phenol also were examined in presence of these titanates.
© 2013 Elsevier Ltd and Techna Group S.r.l. All rights reserved.

Keywords: Layered trititanates; Ion-exchange; Photocatalytic activity; Phenol degradation; Oxidative degradation

1. Introduction

Inorganic layered alkali and alkaline titanates are of considerable interest because of their potential applications. They are used as photocatalysts [1–5], fuel cell electrolytes [6], and cationic exchangers [7], for the treatment of radioactive liquid waste, dielectric resonators in microwave oscillator's band pass [8] and as a reinforcing agent of plastic and adiabatic material [9]. Sodium trititanate ($Na_2Ti_3O_7$), for instance, finds use as ion exchanger, a gas sensor and a ceramic capacitor [10]. A mixture of $Na_2Ti_3O_7$ and $Na_2Ti_6O_{13}$ is used in gas sensors and as reference electrode [11]. These titanates belong to the alkali titanate family with general formula $A_2Ti_nO_{2n+1}$ ($n=3$). Its structure consists of edge and corner shared TiO_6 octahedra in units of $(Ti_3O_7)^{2-}$ layers held together by sodium ions [11] forming rectangular tunnels. Alkali titanates are known to have interesting catalytic, conductive, and ion-exchange properties that depend on their stoichiometry [12].

Ion exchange provides a powerful technique for the removal of toxic substances and the collection of valuable elements from water [13–15]. Fabrication of efficient and cost effective ion exchangers has been studied extensively for recovery of heavy metals from wastewater [16–33] and removal of radioactive waste originating from uranium mining and nuclear accidents. Several inorganic materials such as phosphates [16], synthetic micas [17–19], clay minerals [20], magadiites [21] and titanates [26–33] have been tested to replace the conventional organic resins [34]. Among these materials, titanates are found to be (i) chemically stable, (ii) radiation and temperature resistant and (iii) inexpensive.

The C–H bond activation is one of the major important processes in many applications, starting from the synthesis of fine chemicals in organic chemistry to the industrial conversion of basic building block materials and decomposition of pollutants [35,36]. Catalytic conversion of pollutants into less harmful by products is relatively cheap compared to conventional methods [37]. Some of the efficient copper-based oxidation catalysts have been reported in recent years [38–40]. However these catalysts are expensive and their preparative methods are very lengthy. Thus there is a need to develop photocatalysts for the degradation of organic pollutants. Although the metal insertion in $Na_2Ti_3O_7$ is reported earlier [41,42], their allylic oxidation and photocatalytic activity of organic pollutants have not been reported.

The aim of the present work is to characterize and explore the performance of the ion-exchange process involving Cu^{2+}

*Corresponding author. Tel.: +91 40 276823237; fax: +91 40 27090020.
E-mail address: mugavithal@gmail.com (M. Vithal).

0272-8842/$ - see front matter © 2013 Elsevier Ltd and Techna Group S.r.l. All rights reserved.
http://dx.doi.org/10.1016/j.ceramint.2013.04.025

and Ag^+ with layered type sodium trititanate ($Na_2Ti_3O_7$) and study their (a) catalytic activity against the degradation of methylene blue dye and phenol and (b) catalytic oxidation of cyclohexa-1,4-diene followed by photodegradation of oxidized products under visible light.

2. Experimental

2.1. Preparation of transition metal titanates through ion-exchange method

The powder samples of Cu(II) and Ag(I) doped $Na_2Ti_3O_7$ were synthesized in two stages. *First stage:* Sodium trititanate, $Na_2Ti_3O_7$, (NaTO) was prepared by both sol–gel [43] and hydrothermal methods [44–48]. We have adopted the sol–gel method using titanium metal powder (Sigma-Aldrich), sodium ter-butoxide (Sigma-Aldrich) as the starting materials [49]. All the chemicals were of analytical reagent grade and used without further purification. Titanium metal powder was dissolved separately in H_2O_2 (30 %) and ammonia solution (25%) at 0–5 °C for 4–5 h to form titanium peroxo complex. To this was added an aqueous solution of sodium ter-butoxide in stoichiometric amount with constant stirring. Citric acid (CA) was added to this solution such that the mole ratio of metal ions to CA is 1:2 to obtain the metal in the citrate form. Then the pH was adjusted to about 7 by adding dilute ammonia solution. The mixture was stirred for several hours at room temperature, and the solution was evaporated slowly till a viscous liquid was obtained. At this stage, a gelating reagent, ethylene glycol (EG) was added. The molar ratio of metal ions to EG was kept at 1:2.4. This mixture was digested on a hot plate/stirrer at 100 °C for 2–3 h with constant stirring. The temperature was increased to 160–180 °C at the onset of solidification. The ensuing porous solid mass was ground in an agate mortar and heated at 400 °C in small amounts in an electric burner to remove the organic matter. The obtained black color solid was heated in a muffle furnace at 950 °C for 12 h. The color of the resultant product (NaTO) was white.

2.2. Second stage (ion exchange)

The parent compound, NaTO, was ion-exchanged with a solution of copper (II) chloride and silver nitrate separately to form $CuTi_3O_7$ (CuTO) and $Ag_2Ti_3O_7$ (AgTO) respectively. Typically, 1 g of sodium titanate powder was stirred with 100 mL of 0.1 M $CuCl_2$ ($AgNO_3$) solution at room temperature. The color of the powders was changed to light blue (gray), and the stirring was continued for overnight to ensure complete ion-exchange. The products after ion-exchange were washed with water and dried at 200 °C for 3 h.

2.3. Oxidation of cyclohexa-1,4-diene

1.0 mmol of cyclohexa-1,4-diene was added to a solution containing 3 mL of acetonitrile and 3 mL of water. To this solution 0.2 mol% of a catalyst (NaTO/AgTO/CuTO) was added. Then the reaction mixture was stirred for 8 h at room temperature. The sample of reaction mixture was monitored by liquid chromatography–mass spectrometry (LC–MS), to confirm the formation of hydroquinone and benzoquinone. Subsequently, the reaction mixture was diluted with double distilled water and irradiated with visible light for the photodegradation of hydroquinone and benzoquinone.

2.4. Photodegradation of methylene blue dye

The catalyst (50 mg) was added to an aqueous solution of methylene blue (5×10^{-5} M, 50 mL) in a 100 mL quartz reactor. The photocatalysis experiments were carried out under visible light (300 W Tungsten lamp) for 120 min. Before the light experiments, dark adsorption experiments were carried out for 60 min to attain adsorption–desorption equilibrium. Samples were taken at regular intervals and filtered through the Millipore filter to remove the catalyst particles and analyzed by UV–vis spectrophotometer at $\lambda_{max} = 664$ nm.

2.5. Photodegradation of phenol

The catalyst (100 mg) was added to an aqueous solution of phenol (10^{-4} M, 50 mL) in a quartz reactor. The photocatalysis experiments were carried out under visible light (500 W Tungsten lamp) for 180 min. Dark adsorption experiments were carried out as mentioned above. Samples are taken at regular time intervals and filtered through the Millipore filters to remove the catalyst particles and analyzed by UV–vis spectrophotometer by measuring the optical density at 270 nm.

2.6. Characterization

Thermogravimetric analysis profiles (curves) of all the samples were recorded using Shimadzu differential thermal analyzer (DTG-60H) with a heating rate of 15 °C min^{-1}. SEM-EDS images were recorded on the HITACHI SU-1500 variable pressure scanning electron microscope (VP-SEM). The room temperature X-ray diffractograms of all the samples were recorded using Rigaku miniplex powder X-ray diffractometer (Cu Kα, $\lambda = 1.5406$ Å) in the 2θ range 10–80° for phase confirmation. JASCO V650 UV–vis spectrophotometer was used for UV–vis difffuse reflectance spectra (DRS) measurements in the range 200–800 nm. $BaSO_4$ was used as the reflectance standard. FT-IR spectra were recorded using Shimadzu spectrometer using KBr pellets. The photocatalytic activity of the samples was evaluated by photodegradation of methylene blue (MB) under visible light irradiation of a 300 W Tungsten lamp using HEBER visible annular type photoreactor. In a typical process, 50 mL of aqueous methylene blue (MB) solution with initial concentraion, $C_0 = 5 \times 10^{-5}$ M and 50 mg of catalyst are taken in a cylindrical-shaped glass reactor at room temperature in air and at neutral pH conditions. The suspension was stirred in the dark for 30 min to establish adsorption–desorption equillibrium. At regular time intervals of 20 min, about 3–5 mL of solution was collected and centrifuged to remove the catalyst particles. The change in the concentration of MB was obtained by recording the absorbance at 664 nm

using a JASCO V650 UV–vis spectrophotometer. ^{1}H NMR spectra were obtained on a Bruker AV400 MHz Spectrometer with chemical shifts referenced using the ^{1}H resonance of residual d_6-DMSO. Mass spectra were recorded by the HR LC-MS technique on AccuTOF^{TM} LC Liquid Chromatograph Time-of-Flight mass spectrometer (JEOL, Tokyo, Japan) with a resolution of 8000 (3000) (5% valley definition) as Mass Spectrometry Facility.

3. Results and discussion

3.1. EDS studies

The energy dispersive spectra (EDS) of all the samples are shown in Fig. 1. In the case of NaTO, the area ratio of Na and Ti was found to be close to 2:3. The absence of peak corresponding to Na and the area ratio of Cu and Ti (Ag and Ti) of 1:3 (2:3) in the EDS of CuTO (AgTO) suggest complete exchange of Na^{+} with Cu^{2+} (Ag^{+}).

3.2. XRD analysis

The powder XRDs of the all samples were recorded (Fig. 2). All the diffraction peaks of NaTO are consistent with the reported data (JCPDS no. 72-0148) and free from impurities [6]. The intense peak at $2\theta \approx 10^{\circ}$ corresponding to (100) planes is the lamellar interlayer distance of layered NaTO. In this trititanate, three edge-shared TiO_6 octahedra connect at the corner to form stepped AAAA type $Ti_3O_7^{2-}$ layers [50]. Sodium ions are present in between these layers and are exchangeable with ions and/or neutral molecules as shown in Fig. 3.

The powder XRD patterns of CuTO and AgTO are similar and comparable with the powder pattern of NaTO. A close examination of powder patterns shows a slight shift in the d_{100} lines indicating a change in unit cell parameters. The powder patterns of CuTO and AgTO were least square fitted using the POWD software. The unit cell parameters of NaTO are given as input parameters for least square fitting. Both AgTO and

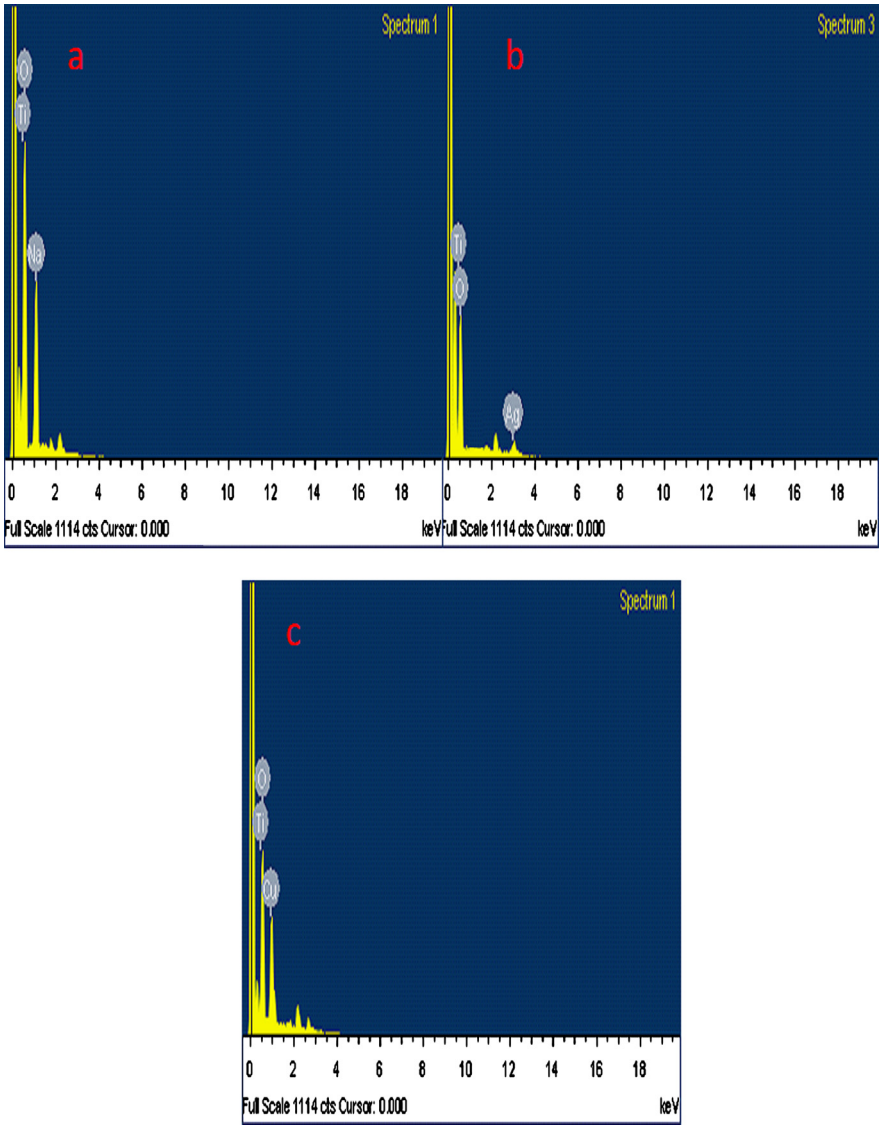

Fig. 1. EDS images of (a) NaTO, (b) AgTO and (c) CuTO.

CuTO also crystallized in monoclinic lattice. The refined unit cell parameters are $a=8.58\pm0.05$ Å, $b=3.79\pm0.05$ Å, $c=9.14\pm0.05$ Å; $\beta=101.58^{\circ}$ for AgTO and $a=8.60\pm0.05$ Å, $b=3.80\pm0.02$ Å, $c=10.81\pm0.02$ Å; $\beta=103.09^{\circ}$ for CuTO. The interlayer separations (d_{100}) of AgTO and CuTO are found to be 0.84 ± 0.02 and 0.79 ± 0.02 nm, respectively.

The crystallite sizes of NaTO, AgTO and CuTO powders were calculated from the line width of intense line (100), using Scherrer's formula:

$$t=\frac{0.9\lambda}{\beta\cos\theta}$$

where t is the thickness in Angstroms (Å) and corresponds to the crystallite diameter assuming a spherical shape, λ is the wave length of the X-ray used, θ is the Bragg angle and β is the full width at half maximum measured in radians of (100) lines in the powder XRD pattern. The crystallite sizes of NaTO, AgTO and CuTO were found to be 40, 32 and 36 nm, respectively (Table 1). The exchange of metal ions into nano-crystallites of NaTO can be attributed to its unique framework structure. The octahedra tunnels running down the b-axis facilitate the diffusion of precursor into the inner parts of the small particles giving rise to homogeneous exchange of metal ions into NaTO lattice.

3.3. Thermogravimertic analysis

Thermogravimetric analysis was carried out to estimate the water content in the titanates. Cu^{2+} doped NaTO did not show

Table 1
Physical properties of all the photocatalysts.

Catalyst	Crystallite size (nm)	Bandgap energy (eV)	% Degradation of MB	% Degradation of phenol	% Oxidation of cyclohexa-1, 4-diene
NaTO	40	3.70	45	13	10
CuTO	36	3.12	86	93	92
AgTO	23	2.98	90	95	98

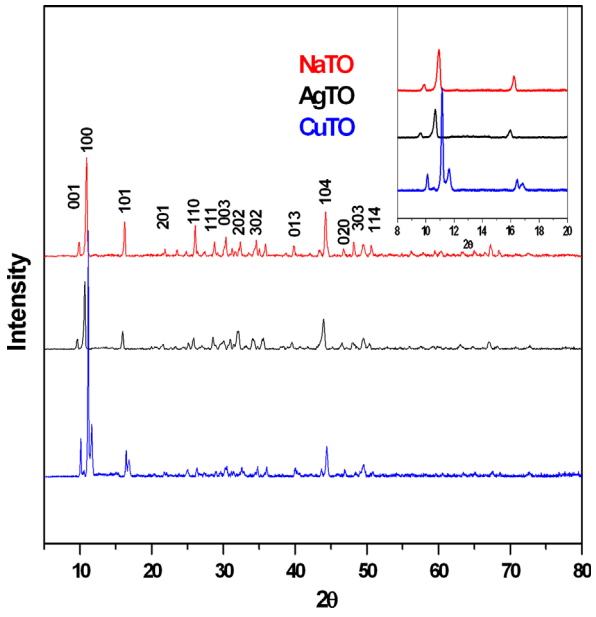

Fig. 2. XRD patterns of NaTO, AgTO and CuTO.

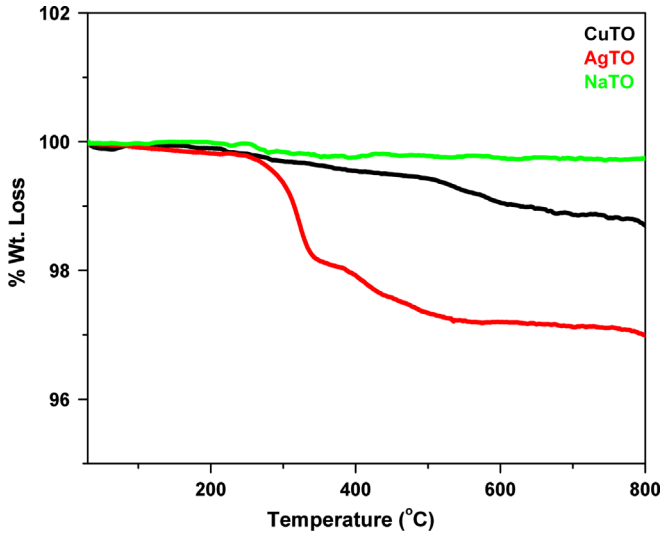

Fig. 4. Thermogram for the matrices NaTO after ion exchange with Cu^{2+} and Ag^{+}.

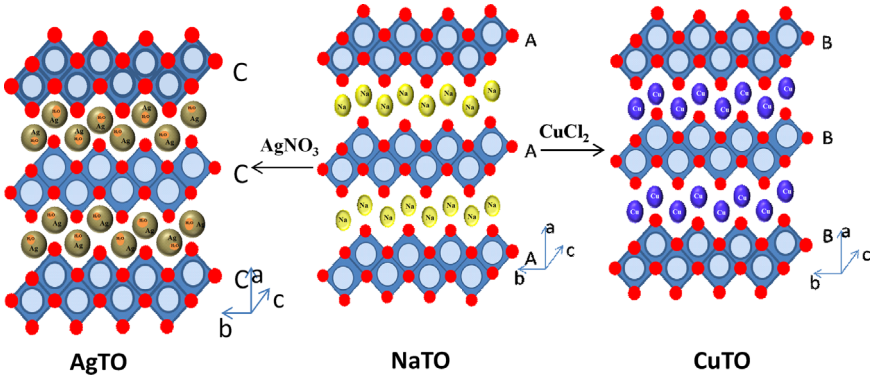

Fig. 3. Model tunnel structures of AgTO, NaTO and CuTO (gray, yellow, blue and orange balls represent Ag^{+}, Na^{+}, Cu^{2+} and H_2O molecules). (For interpretation of the references to color in this figure legend, the reader is referred to the web version of this article.)

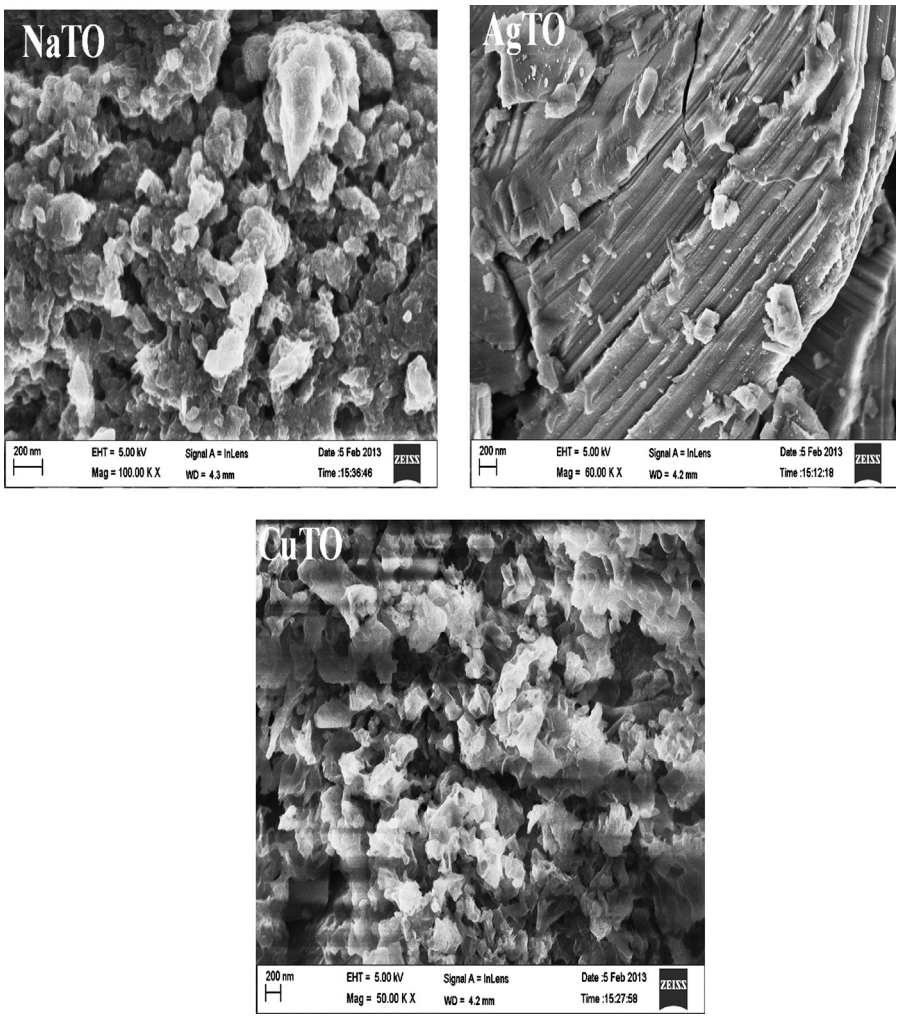

Fig. 5. FESEM images of NaTO, AgTO and CuTO.

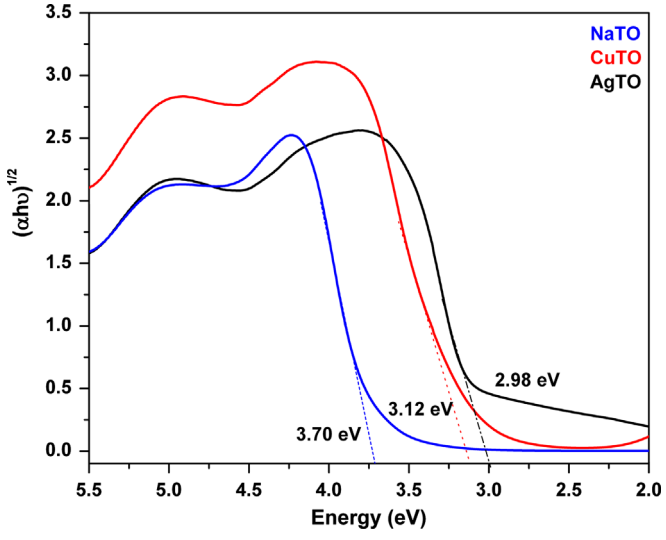

Fig. 6. UV–vis diffuse reflectance spectra of NaTO, AgTO and CuTO.

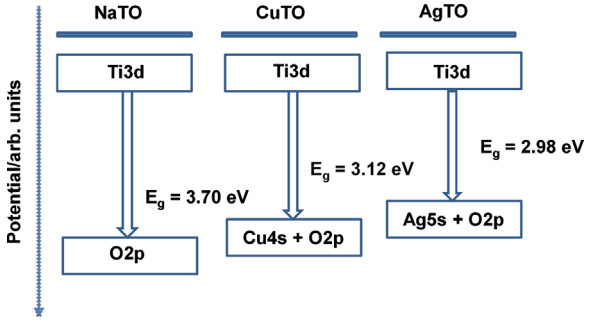

Fig. 7. Proposed energy diagrams of NaTO, AgTO and CuTO.

any weight loss up to 400 °C. On the other hand, Ag^+ doped NaTO has shown a weight loss of 2.5% up to 400 °C (Fig. 4). Based on TGA results, the molecular composition of the titanates can be written as $Na_2Ti_3O_7$ (NaTO), $CuTi_3O_7$ (CuTO) and $Ag_2Ti_3O_7 \cdot xH_2O$ (x=0.2–0.25) (AgTO).

3.4. FESEM analysis

The morphological characterization of NaTO, AgTO and CuTO was obtained from FESEM measurements (Fig. 5). The morphology of all the materials was found to layer type although predominant stacking is clearly seen in AgTO.

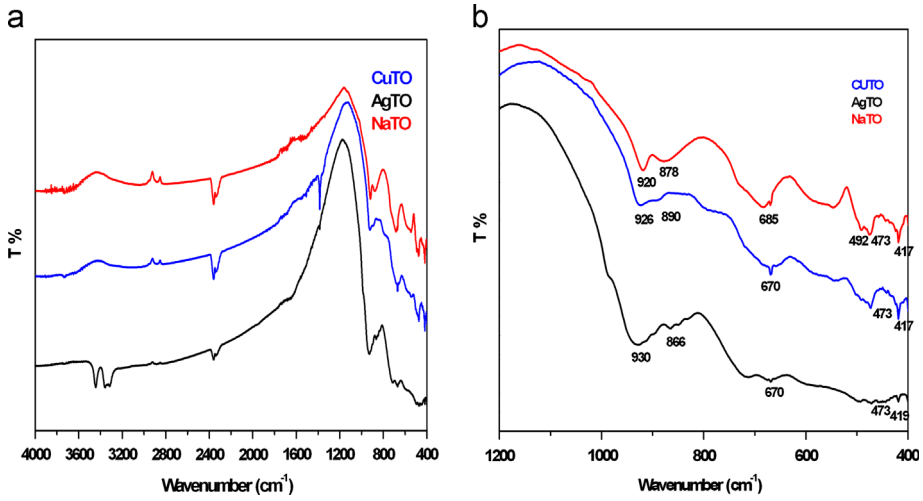

Fig. 8. IR spectra of NaTO, AgTO and CuTO.

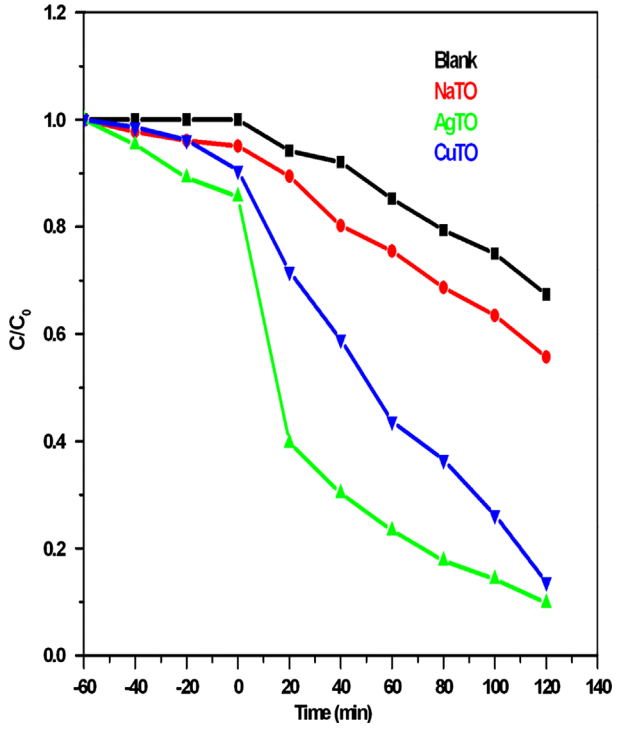

Fig. 9. Degradation of MB in presence of Blank, NaTO, AgTO and CuTO.

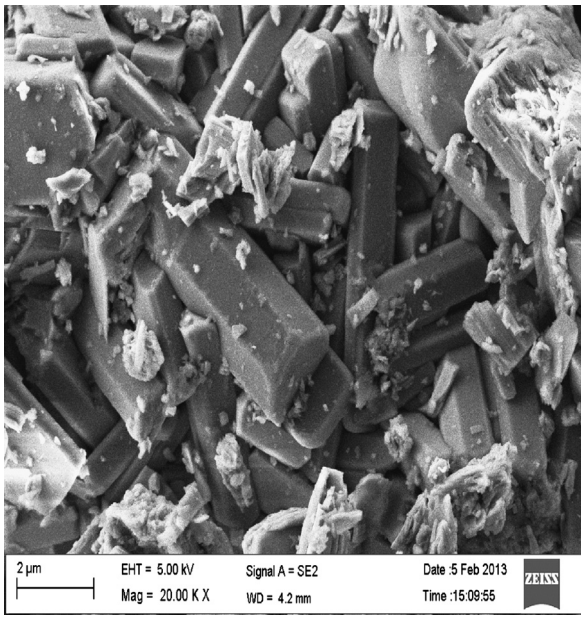

Fig. 10. FESEM image of AgTO nanorods.

3.5. UV–vis analysis

The optical properties of NaTO, AgTO and CuTO powders were obtained from UV–vis diffuse reflectance spectroscopy. These spectra were converted to the absorption spectra by the Kubelka–Munk method [51]. The band gap energy of a semiconductor can be obtained from the plot of $(\alpha h\nu)^{1/2}$ versus $h\nu$, where α is the absorption coefficient and $h\nu$ is the photon energy. In a typical plot, the KM function decreases and becomes almost linear with the x-axis. The perpendicular drawn from the point of intersection of the two straight lines on to the x-axis gives an estimation of band gap energy (see Fig. 6). The band gap energies of NaTO, AgTO and CuTO powders were found to be 3.70, 2.98 and 3.12 eV, respectively (Table 1). Shen et al. have estimated the indirect band gap energy (E_g = 2.99 eV) of NaTO based on DFT calculations [53].

The valence band of this titanate was formed predominantly by O2p orbitals while the conduction band is constituted by Ti3d orbitals [52] (Fig. 7). When Na ions are exchanged with Ag or Cu ions, the 5s orbitals of Ag (4s orbitals of Cu) are mixed with O2p orbitals resulting in an up shift of valence band edge which results in a decrease of band gap energy [53].

3.6. Infra-red spectra

The Fourier Transform Infrared Spectra (FTIR) of all the samples were recorded in the range 4000–400 cm^{-1} and shown in Fig. 8. The IR spectrum of AgTO was characterized by bands in the region 3200–3500 cm^{-1} corresponding to water

which is consistent with TGA results. These bands are absent in the IR spectra of NaTO and CuTO. The bands observed in the region 1200–400 cm^{-1} are similar to each other and comparable with reported spectrum [54]. The bands observed in the range 860–890 cm^{-1} and 920–930 cm^{-1} are due to the stretching vibrations of Ti–O–Ti bonds while the bands in the range 670–685 cm^{-1} and 470–475 cm^{-1} arise due to Ti–O bonds in TiO_6 octahedra [55].

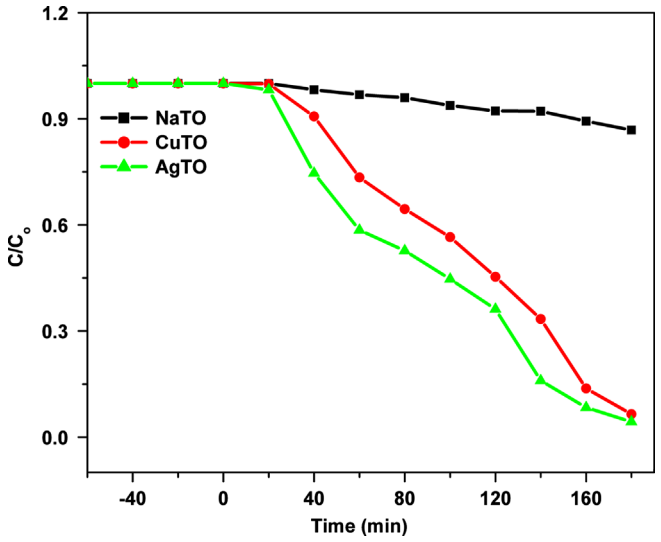

Fig. 11. Photodegradation of phenol in presence of NaTO, AgTO and CuTO.

3.7. Photocatalytic activity

The photocatalytic activity of NaTO, AgTO and CuTO was evaluated by photodegradation of methylene blue (MB) and phenol. The absorption spectrum of MB is characterized by strong overlapping bands at ~600 and 675 nm. These bands were assigned to conjugated π-system [56–58]. The photocatalytic activity of all the samples was monitored by measuring the optical density (OD) at 664 nm and UV–visible spectra at different intervals of light irradiation. It is observed that, the decolorization of MB increases with increase in the irradiation time. The variation of concentration of MB with irradiation time is shown in Fig. 9. The percentage of MB degradation after 120 min was found to be 23%, 90% and 86% for NaTO, AgTO and CuTO respectively (Table 1). It is clear that both AgTO and CuTO show enhanced photoactivity compared to that of NaTO. The photoactivity of a material depends on several factors such as crystallite size of the catalyst, nature of the pollutant, bandgap energy, rate of electron–hole recombination etc. In the present investigation, the higher activity observed for AgTO and CuTO may be due

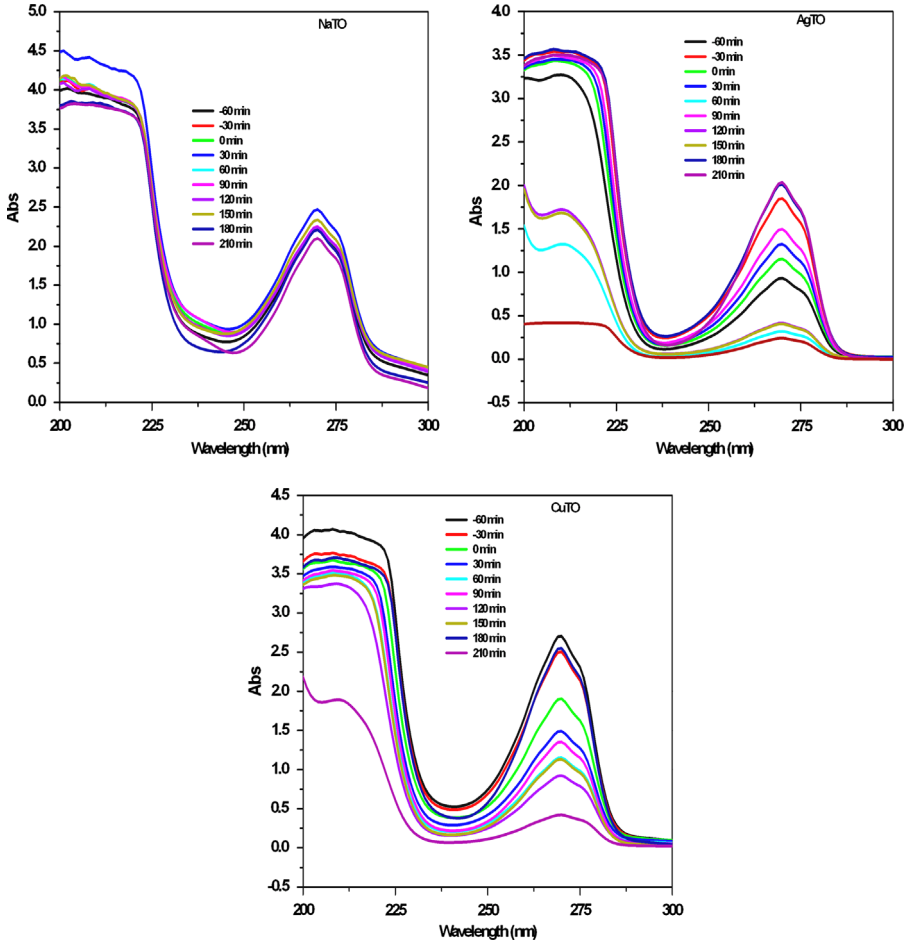

Fig. 12. The absorbance spectra changes of phenol solution in the presence of NaTO, AgTO and CuTO under visible light irradiation.

to (i) newly formed intra-bandgap states close to the conduction band edge to induce electronic coupling which prevents the charge recombination and/or (ii) morphology of the AgTO is nano-rods and each nano-rod consists of several layers (Fig. 10)

We have also examined the photodegradation of phenol in the presence of all the catalysts (NaTO, AgTO and CuTO) and the results are shown in Figs. 11 and 12. The degradation of phenol in the presence of NaTO is very low (about 13%) which may be due to high bandgap value. The photoinduced charges cannot be produced for oxidative degradation of phenol in the presence of NaTO. Under the same conditions, the phenol degradation with CuTO and AgTO was found to be 93% and 95 % respectively in 3 h (Table 1). It is observed that the accumulated holes have a tendency to induce photocorrosion of the catalysts in the presence of phenol [59]. However, in the present investigation, all the catalysts have retained their structure as shown by their powder XRD results.

Klisakova et al. have reported that cyclohexene can be completely decomposed into water and carbon dioxide in the presence of TiO_2 under UV irradiation [60]. In the present investigation, we have studied the degradation of cyclohexa-1,4-diene under visible light irradiation. The proposed mechanism for oxidation of cyclohexa-1,4-diene is shown in Scheme 1 and confirmed from its ^{1}H NMR spectrum. Allylic oxidation of cyclohexa-1,4-diene into dione has been carried out in presence of all the catalysts under ambient conditions according to Scheme 1 and subsequently confirmed by LC–MS. The oxidation reaction was carried out by using different concentrations (0.1–0.5 mol%) of catalysts and 0.2 mol% is found to be an optimal catalyst concentration.

Oxidation of cyclohexa-1,4-diene followed by photodegradation of oxidative products in the presence of all the three catalysts is studied. The first reaction was monitored using ^{1}H NMR and LC–MS techniques. The possible reaction pathway of cyclohexa-1,4-diene into intermediates and their subsequent degradation is shown in Scheme 1. The chromatograms of cyclohexa-1,4-diene solution subjected to oxidation for different intervals of time are shown in Fig. 13. It is observed that the chromatograms are characterized by peaks belonging to parent cyclohexa-1,4-diene and oxidized intermediates (hydroquinone and benzoquinone) up to 6 h of stirring when AgTO and CuTO are used as catalysts. The conversion of parent compound to oxidized products is completed in 8 h (Fig. 14). On the other hand the conversion of parent compound to oxidized products in the presence of NaTO is less even up to

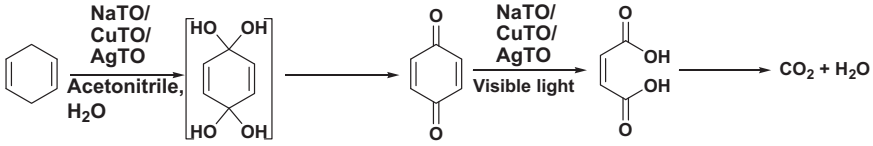

Scheme 1. Photodegradtion pathway of the cyclo-1,4-diene.

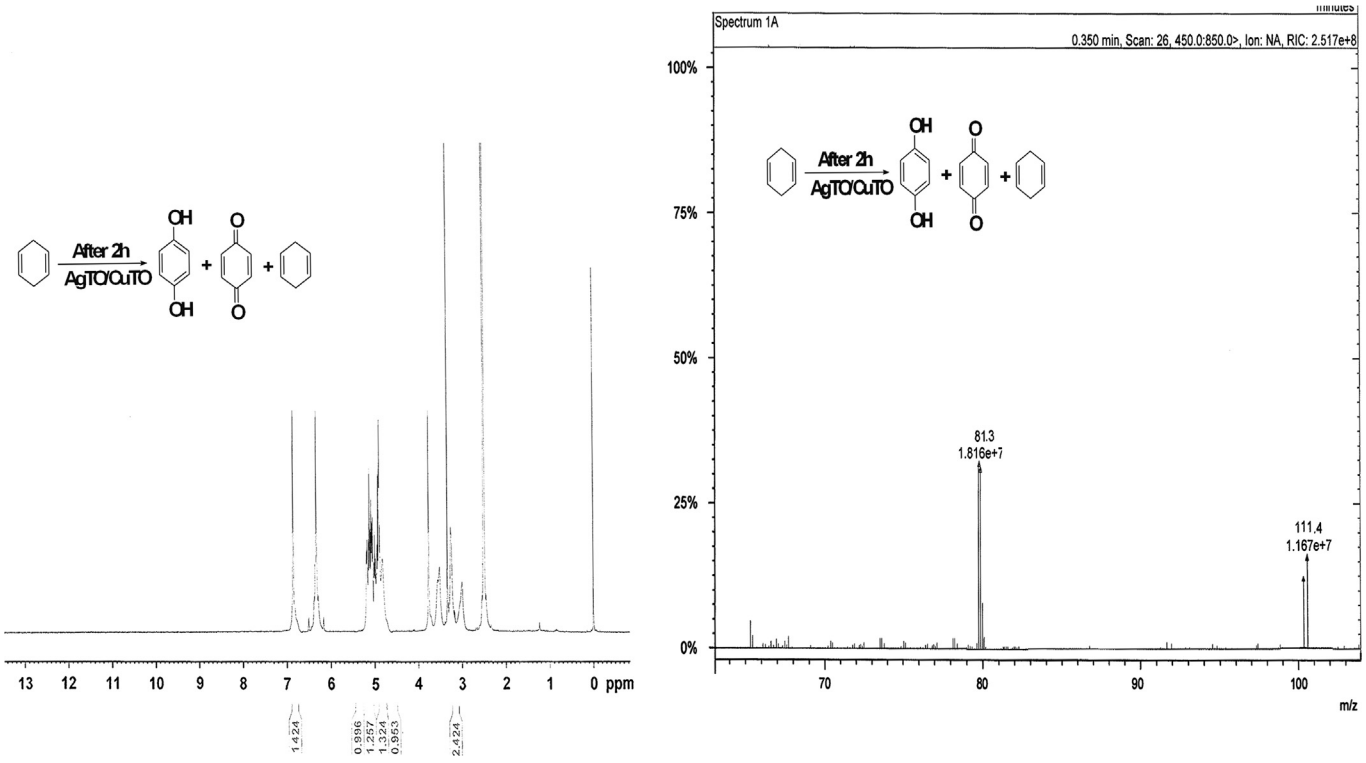

Fig. 13. ^{1}H NMR and LC–MS of oxidation reaction of cyclohexa-1,4-diene in presence of AgTO and CuTO after 2 h.

8 h of stirring. In the second reaction, the oxidized products are subjected to visible light irradiation using tungsten lamp. The oxidized products are mineralized to CO_2 and H_2O in the presence of catalysts (AgTO and CuTO) (Fig. 15).

The mechanism (Scheme 1) of degradation of hydroquinone and benzoquinone [59] is shown below. For the semiconductor photo-catalytic reactions, the generation and separation of the photo induced electron–hole pairs are important factors to determine the efficiency of photocatalyst. Under visible-light irradiation, trititanates are excited to produce photogenerated electrons and holes. The band gap energies of sodium trititanates (E_g=3.70 eV) are more than that of TiO_2 (E_g=3.2 eV), but

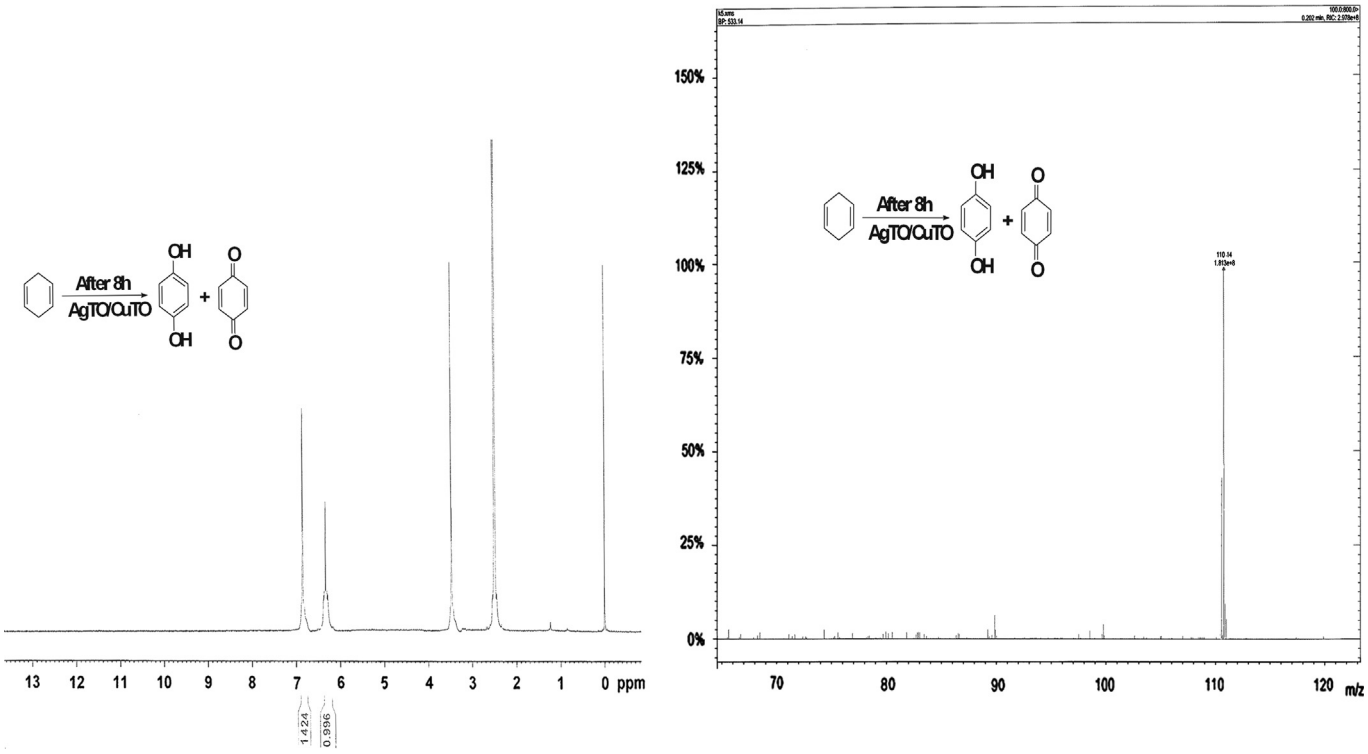

Fig. 14. ^{1}H NMR and LC–MS of oxidation reaction of cyclohexa-1,4-diene in presence of AgTO and CuTO after 8 h.

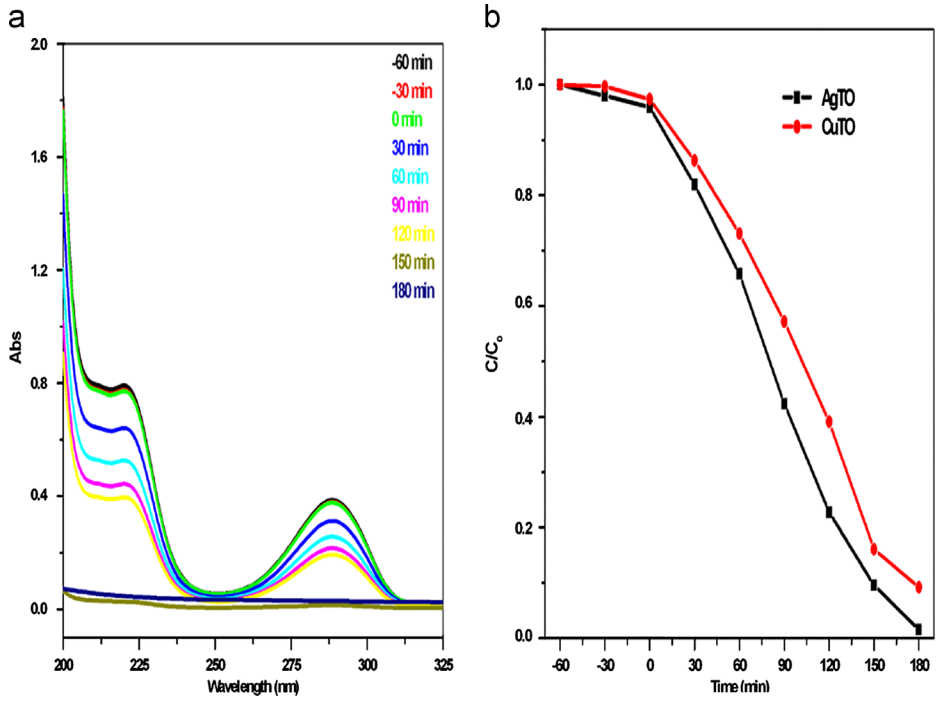

Fig. 15. (A) The absorbance spectra changes of hydroquinone (oxidized products) and (B) photodegradation solution in the presence of NaTO, AgTO and CuTO under visible light irradiation.

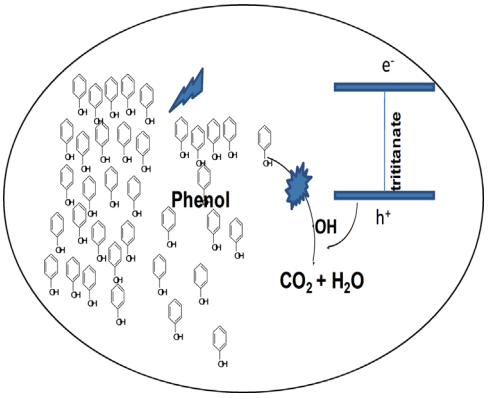

Fig. 16. Probable mechanism of the degradation of phenol on Trititanates.

after ion-exchange with Cu and Ag ions, the band gap energy decreases by about 0.65 eV. The holes generated in the VB of the catalyst oxidize water to form hydroxyl radical ($OH^{\bullet}$), which has strong affinity to oxidize organic pollutant molecules as shown below (Fig. 16). Since the band gap energy of both Cu^{2+} and Ag^{+} exchanged trititanates is less, the photoactivity is expected to be higher than its parent NaTO as observed experimentally.

4. Conclusions

We have successfully synthesized layered trititanates (NaTO, AgTO and CuTO) through a simple sol–gel and ion-exchange procedures. The phase purity and chemical composition of the ion-exchanged samples were well-characterized. The layered crystal structure of CuTO and AgTO were established by POWD analysis using the X-ray powder diffraction data. The obtained layered trititanates CuTO and AgTO have shown high efficiency in photocatalytic degradation of MB and phenol under visible light excitation. Remarkable photocatalytic activity of the layered trititanates can be attributed to their photo induced electron–hole formation and low band gap energy. Both CuTO and AgTO exhibit significant oxidation of cyclohexa-1,4-diene and finally all the intermediates were decomposed into carbon dioxide and water.

Acknowledgments

Authors gratefully acknowledge CSIR—New Delhi (Project no. 03(1199)/II/EMR-II) for financial assistance. SP thanks CSIR —New Delhi for the award of Senior Research fellowship.

References

[1] K.M. Colbow, J.R. Dahn, R.R. Haering, Structure and electrochemistry of the spinel oxides $LiTi_2O_4$ and $Li_{4/3}Ti_{5/3}O_4$, Journal of Power Sources 26 (1989) 397–402.

[2] F. Meng, J. Li, Z. Hong, M. Zhi, A. Sakla, C. Xiang, N. Wu, Photocatalytic generation of hydrogen with visible-light nitrogen-doped lanthanum titanium oxides, Catalysis Today 199 (2013) 48–52.

[3] Z. Li, H. Xue, X. Wang, X. Fu, Characterizations and photocatalytic activity of nanocrystalline $La_{1.5}Ln_{0.5}Ti_2O_7$ (Ln=Pr, Gd, Er) solid solutions prepared via a polymeric complex method, Journal of Molecular Catalysis A: Chemistry 260 (2006) 56–61.

[4] A.G Belous, G.N Novitskaya, S.V Polyanetskaya, Y.I Gornikov, Crystall-chemical and electro-physical characteristics of complex oxides $La_{2/3-x}M_{3x}TiO_3$ (in Russian), Zhurnal Neorganicheskoi Khimii 32 (1987) 283–286.

[5] T. Ohzuku, A. Ueda, J. Yamamoto, Zero-strain insertion material of $Li[Li_{1/3}Ti_{5/3}]O_4$ for rechargeable lithium cells, Journal of the Electro-chemical Society 142 (1995) 1431–1435.

[6] K. Chiba, N. Kijima, Y. Takahashi, Y. Idemoto, J. Akimoto, Synthesis, structure, and electrochemical Li-ion intercalation properties of $Li_2Ti_3O_7$ with $Na_2Ti_3O_7$ type layered structure, Solid State Ionics 178 (2008) 1725–1730.

[7] K. Kunimitsu, A. Junji, K. Norihito, H. Hiroshi, O. Ken-ichi, A. Junji, Ion-exchange synthesis, crystal structure, and electrochemical properties of $Li_2Ti_6O_{13}$, Chemistry of Materials 23 (2011) 2344–2352.

[8] R.D. Adams, R. Layland, M. Danot, C. Payen, A new mixed metal titanate: the synthesis and characterization of $Ba_2Fe_2Ti_4O_{13}$, Polyhedron 15 (1996) 2567–2571.

[9] J.P. Shim, J.S. Lee, H.K. Kee, S.G. Park, The synthesis of potassium hexatitanate and manufacturing alkaline fuel cell matrix, Synthetic Metals 71 (1995) 2261–2262.

[10] V.M. Daskalaki, M. Antoniadou, G.L. Puma, I.K. Dimitris, P. Lianos, Solar light-responsive $Pt/CdS/TiO_2$ photocatalysts for hydrogen production and simultaneous degradation of inorganic or organic sacrificial agents in wastewater, Environmental Science and Technology 44 (2010) 7200–7205.

[11] J. Ramırez-Salgado, E. Djurado, P. Fabry, Synthesis of sodium titanate composites by sol–gel method for use in gas potentiometric sensors, Journal of the European Ceramic Society 24 (2004) 2477–2483.

[12] (a) Y. Inoue, T. Kubokawa, K. Sato, FTIR spectroscopy of UV-generated quinone radicals: evidence for an intramolecular hydrogen atom transfer in ubiquinone, naphthoquinone, and plastoquinone, Journal of Physical Chemistry 95 (1991) 4059–4063;
(b) S. Murugesan, V. Subramanian, Robust synthesis of bismuth titanate pyrochlore nanorods and their photocatalytic applications, Chemical Communications (2009) 5109–5111.

[13] S. Komarneni, R. Roy, Use of γ-zirconium phosphate for Cs removal from radioactive waste, Nature 299 (1982) 707–708.

[14] A.A. Zagorodni, Ion Exchange Materials: Properties and Applications, Elsevier, Amsterdam, 2006.

[15] A.M. Wachinski, J.E. Etzel, Environmental Ion Exchange: Principles and Design, CRC Press, Cleveland, OH, 1997.

[16] B.A. Moyer, Ion Exchange and Solvent Extraction: A Series of Advances, 19, CRC Press, Boca Raton, 2009.

[17] S. Komarneni, R. Roy, A cesium selective ion sieve made by topotactic leaching, Science 239 (1988) 1286–1288.

[18] S. Komarneni, N. Kozai, W.J. Paulus, Superselective clay for radium uptake, Nature 410 (2001) 771.

[19] W.J. Paulus, S. Komarneni, R. Roy, Bulk synthesis and selective exchange of strontium ions in $Na_4Mg_6Al_4Si_4O_{20}F_4$mica, Nature 357 (1992) 571–573.

[20] S.A. Adeleye, P.G. Clay, M.O.A. Oladipo, Sorption of caesium, strontium and europium ions on clay minerals, Journal of Material Science 29 (1994) 954–958.

[21] Y. Ide, N. Ochi, M. Ogawa, Effective and selective adsorption of Zn^{2+} from seawater on a layered silicate, Angewandte Chemie, International Edition 123 (2011) 654–656.

[22] C. Brenan, J. Lovatt, H. Smith, Ion exchange method of estimating strontium-90 and other radionuclides in rainwater, Nature 211 (1966) 68–69.

[23] N. Ding, M.G. Kanatzidis, Selective incarceration of caesium ions by Venus flytrap action of a flexible framework sulfide, Nature Chemistry 2 (2010) 187–191.

[24] A. Dyer, M. Pillinger, J. Newton, R. Harjula, T. Moller, S. Amin, Sorption behavior of radionuclides on crystalline synthetic tunnel manganese oxides, Chemistry of Materials 12 (2000) 3798–3804.

[25] J. Lehto, A. Clearfield, The ion exchange of strontium on sodium titanate $Na_4Ti_9O_{20}\cdot xH_2O$, Journal of Radioanalytical and Nuclear Chemistry 118 (1987) 1–13.

[26] A. Clearfield, J. Lehto, Preparation, structure, and ion-exchange properties of $Na_4Ti_9O_{20} \cdot xH_2O$, Journal of Solid State Chemistry 73 (1988) 98–106.
[27] A.J. Celestian, D.G. Medvedev, A. Tripathi, J.B. Parise, A. Clearfield, Optimizing synthesis of $Na_2Ti_2SiO_7 \cdot 2H_2O$ (Na-CST) and ion exchange pathways for $Cs_{0.4}H_{1.6}Ti_2SiO_7 \cdot H_2O$ (Cs-CST) determined from in situ synchrotron X-ray powder diffraction, Nuclear Instruments and Methods in Physics Research, Section B 238 (2005) 61–69.
[28] M. Nyman, D.T. Hobbs, A family of peroxo-titanate materials tailored for optimal strontium and actinide sorption, Chemistry of Materials 18 (2006) 6425–6435.
[29] M. Poojary, R.A. Cahill, A. Clearfield, Synthesis, crystal structures, and ion-exchange properties of a novel porous titanosilicate, Chemistry of Materials 6 (1994) 2364–2368.
[30] A.J. Celestian, D.G. Medvedev, A. Tripathi, J.B. Parise, A. Clearfield, The mechanism responsible for extraordinary Cs ion selectivity in crystalline silicotitanate, Journal of the American Chemical Society 130 (2008) 11689–11694.
[31] J. Lehto, R. Harjula, A.M. Girard, The equilibrium of strontium ion exchange on sodium titanate, $Na_4Ti_9O_{20} \cdot xH_2O$, Journal of the Chemical Society, Dalton Transactions 1 (1989) 101–103.
[32] D.J. Yang, Z.F. Zheng, H.Y. Zhu, H.W. Liu, X.P. Gao, Titanate nanofibers as intelligent absorbents for the removal of radioactive ions from water, Advanced Materials 20 (2008) 2777–2781.
[33] D.J. Yang, Z.F. Zheng, H.W. Liu, H.Y. Zhu, X.B. Ke, Y. Xu, D. Wu, Y. Sun, Layered titanate nanofibers as efficient adsorbents for removal of toxic radioactive and heavy metal ions from water, Journal of Physical Chemistry C 112 (2008) 16275–16280.
[34] G.L. Hill, E. Bailey, M.C. Stennett, N.C. Hyatt, E.M. Maddrell, P.F. McMillan, J.A. Hriljac, High-pressure and -temperature ion exchange of aluminosilicate and gallosilicate natrolite, Journal of the American Chemical Society 133 (2011) 13883–13885.
[35] S. Caron, R.W. Dugger, S.G. Ruggeri, J.A. Raganand, D.H.B. Ripin, Large-scale oxidations in the pharmaceutical industry, Chemical Reviews 106 (2006) 2943–2989.
[36] T. Punniyamurthy, S. Velusamy, J. Iqbal, Recent advances in transition metal catalyzed oxidation of organic substrates with molecular oxygen, Chemical Reviews 105 (2005) 2329–2364.
[37] A.E. Shilov, G.B. Shulpin, Activation and Catalytic Reactions of Saturated Hydrocarbons in the Presence of Metal Complexes, Kluwer Academic Publisher, Springer, The Netherlands, 2000.
[38] S.I. Chan, C.Y.C. Chien, C.S.C. Yu, P.N. babu, S. Maji, P.P.Y. Chen, Efficient catalytic oxidation of hydrocarbons mediated by tricopper clusters under mild conditions, Journal of Catalysis 293 (2012) 186–194.
[39] Y. Li, T.B. Lee, T. Wang, A.V. Gamble, A.E.V. Gorden, C.–H. Allylic, Activations using Cu(II) 2-quinoxalinol salen and *tert*-butyl hydroperoxide, Journal of Organic Chemistry 77 (2012) 4628–4633.
[40] P.N. babu, S. Maji, M.P. Kumar, P.P.Y. Chen, S.S.F. Yu, S.I. Chan, Efficient room-temperature oxidation of hydrocarbons mediated by tricopper cluster complexes with different ligands, Advanced Synthesis and Catalysis 354 (2012) 3275–3282.
[41] N. Li, L. Zhang, Y. Chen, M. Fang, J. Zhang, H. Wang, Highly efficient, irreversible and selective ion exchange property of layered titanate nanostructures, Advanced Functional Materials 22 (2012) 835–841.
[42] V.A. Cardoso, A.G. de Souza, P.P.C. Sartoratto, L.M. Nunes, The ionic exchange process of cobalt, nickel and copper(II) in alkaline and acid-layered titanates, Colloids and Surfaces A: Physicochemical and Engineering Aspects 248 (2004) 145–149.
[43] Y. Zhang, W. Fu, H. Yang, M. Li, Y. Li, W. Zhao, P. Sun, M. Yuan, D. Ma, B. Liu, G. Zou, A novel humidity sensor based on $Na_2Ti_3O_7$ nanowires with rapid response–recovery, Sensors and Actuators B 135 (2008) 317–321.
[44] A.-L. Sauvet, S. Baliteau, C. Lopez, P. Fabry, Synthesis and characterization of sodium titanates $Na_2Ti_3O_7$ and $Na_2Ti_6O_{13}$, Journal of Solid State Chemistry 177 (2004) 4508–4515.
[45] S. Baliteau, A.-L. Sauvet, C. Lopez, P. Fabry, Controlled synthesis and characterization of sodium titanate composites $Na_2Ti_3O_7/Na_2Ti_6O_{13}$, Solid State Ionics 178 (2007) 1517–1522.
[46] Z. Zhang, J.B.M. Goodall, S. Brown, L. Karlsson, R.J.H. Clark, J.L. Hutchison, I.U. Rehman, J.A. Darr, Continuous hydrothermal synthesis of extensive 2D sodium titanate($Na_2Ti_3O_7$) nano-sheets, Dalton Transactions 39 (2010) 711–714.
[47] Y.V. Kolenko, K.A. Kovnir, A.I. Gavrilov, A.V. Garshev, J. Frantti, O.I. Lebedev, B.R. Churagulov, G. Van Tendeloo, M. Yoshimura, Hydrothermal synthesis and characterization of nanorods of various titanates and titanium dioxide, Journal of Physical Chemistry B 110 (2006) 4030–4038.
[48] M. Milanović, I. Stijepović, L.M. Nikolić, Preparation and photocatalytic activity of the layered titanates, Processing and Application of Ceramics 4 (2010) 69–73.
[49] B.V. Kumar, R. Velchuri, V.R. Devi, G. Prasad, B. Sreedhar, C. Bansal, M. Vithal, Preparation, characterization, emission (Eu^{3+}), and electron spin resonance (Gd^{3+}) studies of $Y_{2-x}Ln_xTi_2O_7$ (Ln = Eu and Gd, $x = 0.0$, 0.05), Journal of Applied Physics 108 (2010) 044906-1–044906-9.
[50] M. Mori, Y. Kumagai, K. Matsunaga, I. Tanaka, First-principles investigation of atomic structures and stability of proton-exchanged layered sodium titanate, Physical Review B 79 (2009) 144117-1–144117-6.
[51] K. Maeda, T.E. Mallouk, Comparison of two- and three-layer restacked Dion–Jacobson phase niobate nanosheets as catalysts for photochemical hydrogen evolution, Journal of Material Chemistry 19 (2009) 4813–4818.
[52] Y. An, Z. Li, H. Xiang, Y. Huang, J. Shen, First-principle calculations for electronic structure and bonding properties in layered $Na_2Ti_3O_7$, Central European Journal of Physics 9 (2011) 1488–1492.
[53] M. Machida, X. Wei Ma, H. Taniguchi, J. Yabunaka, T. Kijima, Pillaring and photocatalytic property of partially substituted layered titanates, $Na_2Ti_{3-x}M_xO_7$and $K_2Ti_{4-x}M_xO_9$ (M = Mn, Fe, Co, Ni, Cu), Journal of Molecular Catalysis A: Chemistry 155 (2000) 131–142.
[54] A.V. Kostrikin, F.M. Spiridonov, I.V. Lin'ko, B.E. Zaitsev, O.V. Kosenkova, S.V. Tarasova, L.N. Komissarov, Interaction of components in the NaOH–TiO_2 H_2O–H_2O system at 25 °C, Russian Journal of Inorganic Chemistry 56 (2011) 928–934.
[55] F.G. Vilchez, W.P. Griffith, Transition-metal tetra-oxo-complexes and their vibrational spectra, Journal of the Chemical Society, Dalton Transactions (1972) 1416–1421.
[56] G. Ravi, S. Palla, J.R. Reddy, N.K. Veldurthi, B.V. Kumar, M. Vithal, Photocatalytic and conductivity studies of Bi^{3+}Substituted $La_2Zr_2O_7$, International Journal of Green Nanotechnology 4 (2012) 360–367.
[57] S.K. Cushing, J. Li, F. Meng, T.R. Senty, S. Suri, M. Zhi, M. Li, A.D. Bristow, N. Wu, Photocatalytic activity enhanced by plasmonic resonant energy transfer from metal to semiconductor, Journal of the American Chemical Society 134 (2012) 15033–15041.
[58] F. Meng, Z. Hong, J. Arndt, M. Li, M. Zhi, F. Yang, N. Wu, Visible light photocatalytic activity of nitrogen-doped $La_2Ti_2O_7$ nanosheets originating from band gap narrowing, Nano Research 5 (2012) 213–221.
[59] Y. Wang, Y. Zhang, G. Zhao, H. Tian, H. Shi, T. Zhou, Design of a novel Cu_2O/TiO_2/carbon aerogel electrode and its efficient electrosorption-assisted, ACS Applied Materials and Interfaces 4 (2012) 3965–3972.
[60] J. Klisakova, P. Kluson, L. Cerveny, Photocatalytic Oxidation of Cyclohexene on Titanium(IV) Oxide, Collection of Czechoslovak Chemical Communications 68 (2003) 1985–1997.